Experiments in Quadrotor Formation Flying Using On-Board Relative Localization

Ioannis Rekleitis[‡], Philippe Babin[†], Andrew DePriest[‡], Sourav Das[‡], Olivier Falardeau[†],
Olivier Dugas[†], and Philippe Giguère[†]

Abstract— Formation flying of aerial robots has many applications, such as surveillance, coordinated transport of heavy objects, convoying, and others. Current research on formation control often relies on the use of an external motion capture equipment to track the pose of each individual robot. In order to deploy multiple Unmanned Aerial Vehicles (UAVs) to arbitrary environments, an alternative to motion capture or differential GPS is needed. In this paper, we show a proof of concept of a bearing-only relative localization approach in the context of maintaining flying formations, by recovering the 6 Degree of Freedom (DoF) relative pose between a pair of flying vehicles. This relative pose, estimated from a pair of images from mutually observing robots, is directly used to guide a follower quadrotor to keep a fixed position with respect to a leader. Experimental results from indoor and outdoor flying of two off-the-shelf quadrotors (Parrot *AR.Drone* 2.0) are presented.

I. INTRODUCTION

Recent years have seen great advances in the use of multiple UAV's especially quadrotors [1]. Work on aggressive manoeuvring [2] multi-UAV grasping [3], synchronized flying following the music [4], [5] and even pole throwing and catching [6], has demonstrated the agility and capabilities of this recently developed platform. A common thread in these results is the presence of a motion capture system such as *Vicon* or *OptiTrack* that enables very high precision tracking of the position and attitude of the flying vehicles. Such reliance limits the application domain to indoor, instrumented spaces.

Similarly to others [7]–[13], we wish to explore the use of on-board cameras to perform relative localization in order to remove the need for an external motion capture system. More specifically, this paper reports on formation-flying experiments for a pair of inexpensive quadrotors, utilizing bearing-only measurements from two monocular cameras, to recover the 6 degree of freedom (DoF) relative pose.

Our demonstration of formation flying with off-the-shelf flying vehicle and under the Robot Operating System (i.e. ROS on *AR.Drone 2.0*) is based on the 6DoF Cooperative Localization proposed by Dugas et al. [14], itself an extension of a 3DoF algorithm proposed earlier by Giguere

[†]P. Babin, O. Falardeau, O. Dugas, and P. Giguere are with Département d'informatique et de génie logiciel, Université Laval, Québec, QC, Canada G1V 0A6. philippe.giguere@ift.ulaval.ca, philippe.babin.1@ulaval.ca

[‡]I. Rekleitis, A. DePriest, and S. Das, are with the Computer Science and Engineering Department, University of South Carolina, Columbia, SC, 29208, USA [sdas,depriesa]@email.sc.edu, yiannisr@cse.sc.edu

Fig. 1. Two quadrotors *AR.Drone* flying in formation. This was the vehicle type used in our experiments.

et al. [15]. Additionally, this paper includes the automatic detection of visual markers (as opposed to manual detection in our previous work) and false positive rejection through a unique feature of our localization technique (the ability to compute the solution in two independent ways). We tested formation flying with two quadrotors in both indoors and outdoors environment. The leader quadrotor used the parallel tracking and mapping PTAM [16] implementation[1] based on ROS [17]–[19] to perform a variety of maneuvers. In the presented setup, PTAM was used only to stabilize the flight of the leader and was successfully used even during rotations. Several different flight patterns were used to test the effectiveness of our approach for formation flying, including motion along the different axis (up/down, left/right, forward/backward), rotations in place, and finally, a helical pattern (rotation and simultaneous vertical translation).

The following Section II discusses related work. Section III provides a brief outline of the bearing only cooperative localization and the practical considerations that arise from the deployment on the *AR.Drone* 2.0. Experimental results from two UAV's flying in formation are presented in Section IV, together with an evaluation of the accuracy of the proposed setup. We conclude this paper with lessons learned and a discussion on future work.

II. RELATED WORK

Computing the relative pose of a team of robots was introduced in 1994 [20]. Initial work focused on 2D pose estimation for localization [21] and mapping [22], using either a Kalman [23], [24] or a Particle [25] filter. Anonymous measurements were utilized in [26]. More recently,

work on using bearing only (monocular) measurements produced an accurate solution for the 2D case [15]. Zhou and Roumeliotis presented a extensive list of solutions for Cooperative Localization in 3D [27] using combinations of range and bearing measurements in conjunction with ego-motion measurements [28]–[30].

The precision of vision-based methods for calculating distance is limited, mainly due to discretization errors. However, systems have been developed to improve the precision using measurements of orientation as cameras act as good protractors. For instance, bearing measurements were used in [31] to estimate the configuration parameters of a continuum robot. Also, implicit localization methods were presented with bearing-only measurements in [32]. Polynomial solvers were developed and optimized for solving minimal geometry problems [33].

Closer to our work of performing full 6-DoF relative localization for flying vehicles using monocular cameras, [7] tracked the relative pose between two fixed-wings vehicles using a Kalman Filter, based on the location in the follower's camera of three key points of the target airplane (center, left and right wingtips). Recently, focus has shifted on using dedicated markers on rotary-wings (quadrotors) aircrafts to perform relative localization. One way is use fiducial markers with significant surface area, such as circular markers [8], [9] or ARToolkit tags [10]. Distance and orientation are estimated from the shape (deformation), in the image plane, of these markers. Another approach is to attach a collection of point-like markers (passive or active) on UAVs; then a number of mathematical formulations can be employed to recover the full 6 DoF pose. For instance, it can be done by solving a perspective-3-point (P3P) problem [11]–[13]. For these works, they have specific markers arrangements: Faessler et al. [11] proposed using at least 4 infrared LEDs, placed in such a way as to span a large volume in order to minimize pose uncertainty. Wenzel et al. [12] used 3 non-collinear infrared LEDs that are detected by the camera of a Nintendo Wii remote mounted on a pan-tilt unit onboard the vehicle, while Lugo et al. [13] used 3 non-collinear table tennis balls tracked with a monocular camera.

The methods in the previous paragraph extracted the relative pose from a single image. However, it is also possible to recover this 6 DoF relative pose by instead employing a *pair* of images that have been captured simultaneously by the vehicles; the constraint is that they have to be mutually observing, *i.e.* markers of *A* must be visible in the image captured by *B*, and vice-versa. A numerical solution was proposed for estimating the 6 DoF relative pose using this approach [34], whereas we proposed one that has a closed-form approximate solution [14], [15], albeit with some constraints on the location of the markers. Additionally, our approach only requires the use of 2 markers per vehicle.

III. RELATIVE POSE ESTIMATION

Our implemented approach [14], [15] has been designed from the ground-up to be applicable to the relative localization problem of lightweight UAVs. In particular, it relies

on a limited number of markers (2 per UAV), placed in a collinear or near-collinear manner with the on-board camera. This configuration is particularly well-suited for UAVs, since they tend generally to be flat-shaped. When flying at similar or near similar altitude, these UAVs will have a good side-view of each others. An overview of our technique is found in the rest of this Section; we refer the reader to [14] for a more detailed description of the approach.

A. 6DoF Bearing only Cooperative Localization

The 3D cooperative localization problem is depicted in Fig. 2, and can be described as follows. A pair of UAVs, $Robot_A$ and $Robot_B$, are free to move in all 6 DoF. Each $Robot_i, i \in \{A, B\}$ is equipped with a single camera and two visual markers. These two markers, R_i and L_i, are placed at a distance d from each other, with the center of projection of the camera located exactly between these markers (a more generic solution is described in [14]). The relative distance l between $Robot_A$ and $Robot_B$ can be estimated directly from two images (I_A taken by $Robot_A$ and I_B taken by $Robot_B$) recorded at the same time. From these two images, we extract two angles α and β:

- from image I_B: $\alpha = \widehat{L_A C_B R_A}$, which is the angle formed between the markers of $Robot_A$ and camera C_B;
- from image I_A: β, the angle between the optical axis of C_A and the ray passing through the origins of C_A and C_B, where the position of C_B is approximated from the location of L_B and R_B.
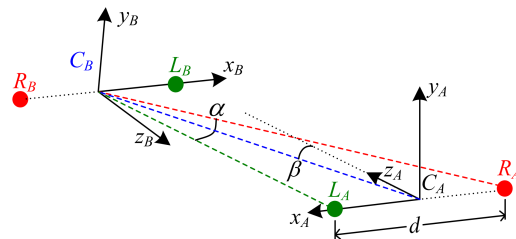

Fig. 2. The relative localization problem in 3D, for the two robots *A* and *B* operating in 6 DoF. The red and green dashed lines represent the ray between the markers on robot *A* and the center of projection C_B. The α angle is computed between these rays. The blue dashed line represents the estimated ray between C_B and the center of projection C_A. The angle β is computed between the optical axis z_A of camera *A* and this ray.

With these angles α and β and the a-priori known distance d between the markers on a vehicle, a closed-form solution yields the distance $l = |C_A C_B|$ between the cameras [15]:

$$ l = \frac{d}{2 \sin \alpha} \left(\cos \alpha \cos \beta + \sqrt{1 - \cos^2 \alpha \sin^2 \beta} \right). \quad (1) $$

Moreover, sufficient information is contained in the two images I_A and I_B to recover uniquely and rapidly the relative orientation between the two vehicles, via simple axis-angle rotation estimations. The error on such estimation is directly proportional to the angular error of the camera, and not the distance l. This is in contrast to [11], where the angular orientation error increases as a function of the distance.

B. Image Processing and Outlier Rejection

For our experiments, each quadrotor was fitted with two colored markers, collinear with the front facing camera. Each of these markers consisted of an orange marker above and an orange marker below the protective frame of the vehicle, as shown in Figs. 1 and 3. These colors were selected as to be distinct from the environment, thus reducing the potentially large number of false markers.

The marker detection pipeline (done in OpenCV) first subtracts the grey-scale value from the red channel (using the HSV color space resulted in too many false positives). Then dilation followed by erosion is performed, resulting in each of the two closely-spaced markers to merge into a single blob. Contours are then calculated and blobs that were too big, or when the vertical-to-horizontal ratio was outside a threshold were eliminated, similarly to [11]. Figure 3 shows the views as captured by the cameras of the two quadrotors, together with the output of the vision pipeline showing the detected marker poses; close-up of the two UAV's and the detected markers can be seen as well.

A final verification test, unique to our approach, was then performed between all possible combinations of pairs of markers in I_A and I_B. As mentioned earlier, the distance l can be computed in two ways: either by extracting α from 2 candidate markers I_B and β from the average (mid-point) of 2 markers' candidate in I_A, or by doing the converse. If both estimates of l are reasonably close, then the marker pairs used in these computations were considered as valid. Since l in Eq. 1 is a closed-form solution, it can be computed rapidly (less than 300 ns on a standard computer.) If more outliers were present in images, long-term filtering and actively tilting one of the vehicle could be employed to mitigate the situation.

Note that for the sake of simplicity, we assume that the images are time-stamped on each vehicle, and that their respective clocks have been synchronized beforehand. In worst case, a clock synchronization protocol such as *Chrony* could be run in the background, or the GPS clock signal themselves used as timestamps if the vehicles are outdoor. We also assume perfect communication between the UAVs, as they are at close range.

IV. EXPERIMENTAL RESULTS

A. Experimental Setup

We used two off-the-shelf *Parrot AR.Drones 2.0* for our experiments. The ROS interface was based on the `ar-drone` autonomy package [35]. Experiments were performed successfully outdoors over long distances, in a setup similar to the one shown in Fig. 1. However, in order to verify the accuracy of our approach, we performed a series of experiments indoors. Note that the emphasis of these experiments is not on the actual precision of the technique (as it has been previously established in [14], [15]), but rather on the feasibility of formation flying using our technique on actual *AR.Drones 2.0* hardware.
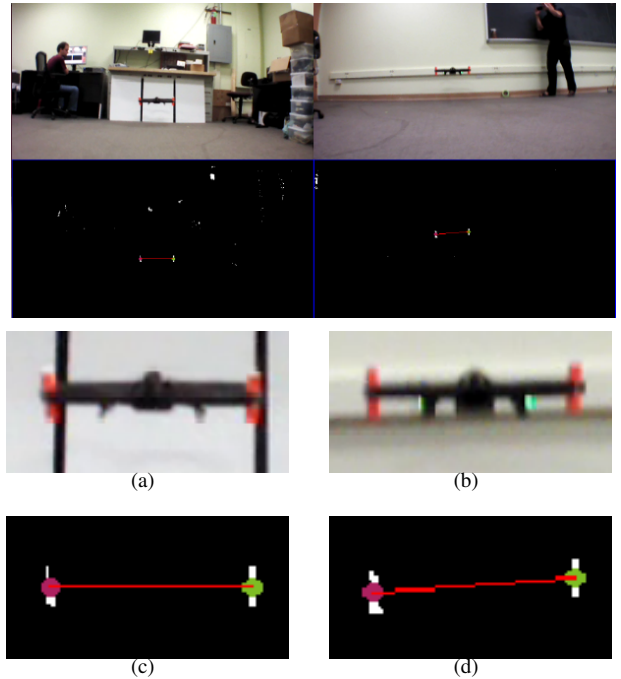

Fig. 3. (a) Screen capture of the images from the two cameras together with the marker detections. (b,c) Close-up of the two quadrotors. (d,e) the markers detected connected with a line each.

B. Flight Formation

In the following tests, formation flying of 2 quadrotors was based on a leader/follower paradigm. The leader quadrotor was flown autonomously using commands sent from a remote machine, with the PTAM state estimation package [16] used to track its position. The TUM *AR.Drone* ROS based package[2] was used to control the leader as well as the follower. The relative position of the follower was computed using our approach described in Sec. III; this pose was used as the input of the TUM *AR.Drone* controller running on the follower. The target relative position of the follower in most of the experiments was $\mathbf{x} = [0, l_{target}, 0]^T$, meaning that the robot should always stay in front of the leader at a distance l_{target}, and at the same altitude; see Table I for the different distances used in the presented experiments. The relative orientation was set to $\mathbf{q} = [0, 0, -180°]^T$, which means that the follower should always face towards the leader.

C. Leader Flight Test Patterns

Several different test trajectory patterns of the leader were used to validate the cooperative localization based formation flying; please refer to Table I for a list of the experiments and Fig. 4 for representative examples. An axis pattern (A1-A5)[3] which comprised of a number of short, straight motion around the origin of the global coordinate system, such as the leader moving up then down, moving forward/backward, then left-right lateral motions; see Fig. 4a. These patterns were always centered around the origin, and were primarily designed to test the ability of the follower to maintain the

---

[2]http://wiki.ros.org/tum_ardrone
[3]The labels A1, R1, etc. are used to label the different experiments; see Table I for a short description.
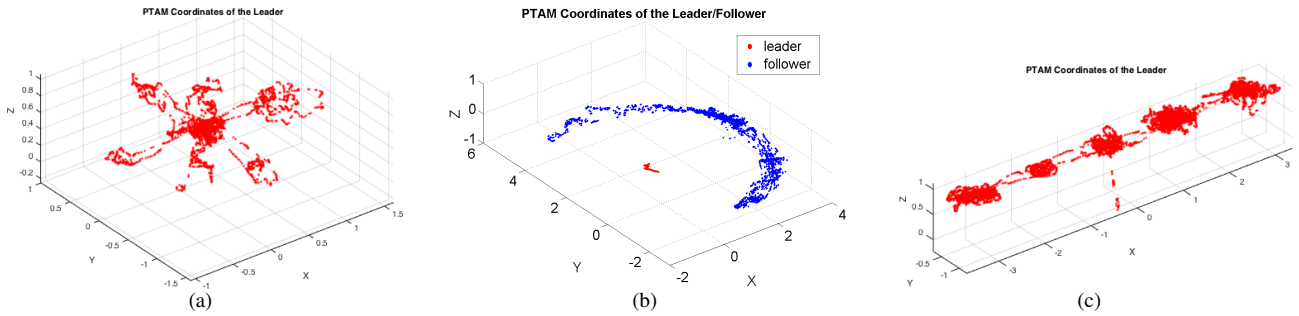
Fig. 4. (a) Flying along the coordinate axis, up/down, forward/backward, left/right. Always returning to the center position (A5). (b) Rotation by $180°$, (R1). (c) Long Lateral motion (L1).

TABLE I
LIST OF EXPERIMENTS AND SEPARATION DISTANCE (d) BETWEEN THE TWO DRONES.

Exp.	l_{target} (m)	Description
A1	2.7	Inside, Axis pattern (1 m each direction). PTAM used
A2	2.7	Inside, Axis pattern (1 m each direction). PTAM used
A3	2.7	Inside, Axis pattern (1 m each direction). PTAM used
A4	2.7	Inside, Axis pattern (1 m each direction). PTAM used
A5	3.7	Outside, Axis pattern (1 m each direction). PTAM used
R1	3.7	Outside, leader on a base, manually rotated, following a $\pm90°$ arc. PTAM not used
R2	3.7	Outside, leader on a base, manually rotated, following a $\pm40°$ arc. PTAM used
R3	2.0	Inside, leader flying, following a $\pm50°$ arc. PTAM used
L1	3.7	Inside, long lateral motion $\pm3m$ each side. PTAM used
M1	2.7	Inside, tele-operated inside an 1 m cube. PTAM used
M2	3.7	Outside, tele-operated to rotate $360°$. Small lateral adjustments to avoid collisions. PTAM used, lost track

fixed distance l_{target} between the vehicles, in the absence of significant orientation change. Changes in the orientation (with respect to global frame) were also tested, by rotating the leader in place, thus forcing the follower to follow an arc trajectory to maintain a constant distance and relative orientation (i.e. rotating to always face the leader). Figure 4b illustrates the yaw rotation pattern, where the leader position was kept nearly steady but was rotated around its z-axis. For these tests, three different rotations were performed (R1-R3). Longer flight patterns were also used. Figure 4c shows a flying test pattern (L1) where the leader flew a longer lateral motion than previous tests, and the follower was required to keep up with the leader. Thus, the follower had to perform similar left or right motions in the global coordinate system, while keeping up with the leader as it reversed direction.

D. Test Results

Figure 5 presents experimental results from three representative runs. All three subfigures have the same structure. The lateral displacement is plotted in the first subplot. For example, in Fig. 5c the leader flew to the right for 3 m then to the left then back to center, and the follower (red line) kept track. In Fig. 5b, as the leader rotated in place, the follower change its lateral position to follow the arc that can be seen in Fig. 4b. The second subplot from the top, refers to the distance between the two robots. In subfigure 5a the leader, after an up/down motion, moved forward and the

follower responded accordingly, approximately at the 130 s. The third subplot display the altitude of the two quadrotors, Fig. 5a illustrates an ascent followed by a descent at the first section of the plot. Finally, the bottom subplot presents the Euclidian error between the desired and recorded position.

The results from several experiments were combined in two tables (II , III). The first Table II presents the root mean square error for the position (in meters) and orientation (in degrees) along the different coordinates. The position of the robot exhibited error around half a meter on average and the orientation about five degrees. We attribute this error predominantly to the inability of the PID controller and of the quadrotor itself to respond to sudden changes in direction, which resulted in overcompensation. This becomes clear as on average, the follower kept within a few cm from the desired position; see Table III. The average orientation was two to three degrees off zero for the roll and pitch and three degrees from the desired $180°$.

E. Challenges

The use of two-low cost quadrotors for formation flying in the context of relative localization presented several challenges. Indeed, the lower quality and reaction time of the on-board sensors and actuators will limit the final achievable precision of the system. Inherent to all quadrotors are the various aerodynamic effects that perturb the system, such as air current or ground/wall effects. Some loss of precision is also due to the various controllers and position trackers (not related to our relative localization technique) employed in this formation. More specifically, the leader maintains a target position by relying on the PTAM-based self localization. As such, the true position of the leader changes constantly due to PTAM localization errors. Moreover, the PID controller used to control the leader and follower were not perfectly tuned or were limited in response time, resulting in lag or ringing with abrupt command changes. For example during the lateral motion the follower lags behind, and then when the leader reverses its direction, the follower overshoots by a certain amount. Finally, the leader needs to pitch or roll during motion, resulting in a tilting of its reference frame compared to the global frame. Proper formation keeping needs to ignore theses changes in orientation and maintain a fixed position with respect to the center of the leader and a gravity-aligned reference frame. While this was explicitly
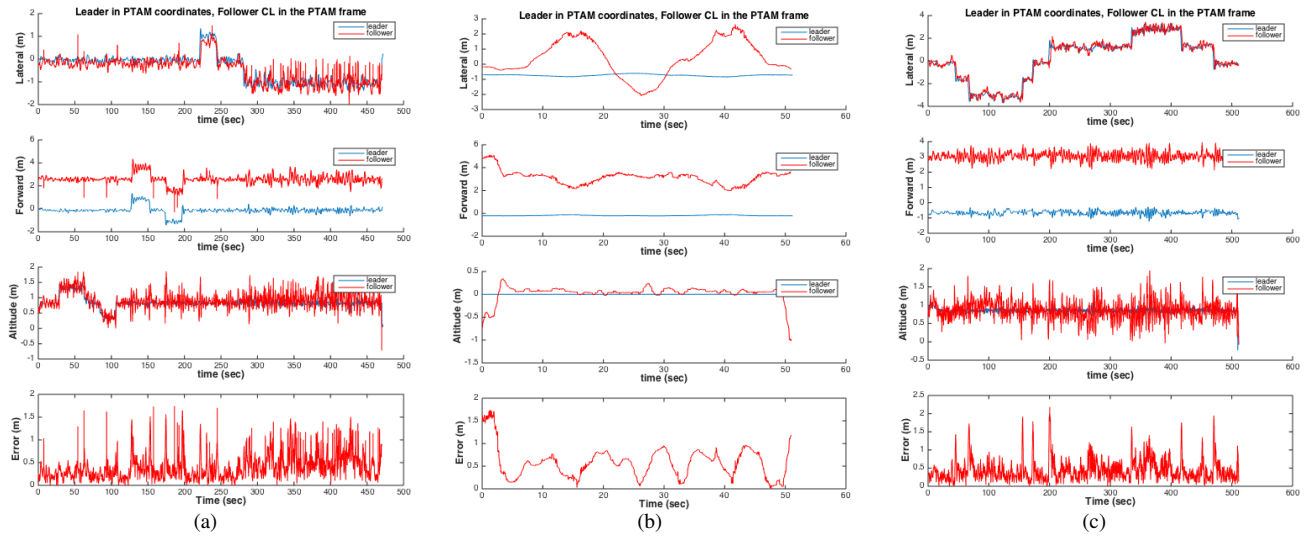
Fig. 5. A subfigures: Top subplot: lateral position of the leader and the follower; second from top: forward position leader/follower; second from bottom: elevation of leader/follower; bottom subplot: Euclidian error of CL. (a) Motion along the axis pattern; see fig. 4a. (b) 180° rotation; see fig. 4b. (c) Lateral motion; see fig. 4c.

TABLE II

THE ROOT MEAN SQUARE ERROR FOR DIFFERENT EXPERIMENTS

Exp.	RMS (x)	RMS (y)	RMS (z)	RMS (roll)	RMS (pitch)	RMS (yaw)	Remarks
A1	0.35 m	0.44 m	0.19 m	6.04°	4.98°	4.98°	Inside axis
A2	0.32 m	0.40 m	0.20 m	6.97°	5.62°	4.66°	Inside axis
A3	0.34 m	0.37 m	0.19 m	5.36°	5.13°	4.23°	Inside axis
A4	0.26 m	0.33 m	0.22 m	5.30°	6.22°	3.70°	Inside long axis
A5	0.28 m	0.34 m	0.24 m	4.94°	4.55°	4.44°	Outside axis
R1	0.54 m	0.18 m	0.11 m	4.52°	2.50°	5.27°	Outside rotation (180°)
R2	0.52 m	0.40 m	0.19 m	4.67°	2.60°	5.24°	Outside rotation (80°)
R3	0.29 m	0.31 m	0.14 m	6.91°	5.61°	5.57°	Inside rotation (100°)
L1	0.36 m	0.31 m	0.20 m	6.14°	5.73°	2.81°	Inside lateral motion
M1	0.30 m	0.26 m	0.17 m	3.50°	5.07°	1.93°	Inside manual motion
M2	0.40 m	0.23 m	0.22 m	5.12°	4.73°	3.63°	Outside manual motion (360° spiral)

TABLE III

AVERAGE POSE FOR DIFFERENT EXPERIMENTS

Exp.	x		y		z		roll		pitch		yaw	
	mean(x)	σ_x	mean(y)	σ_y	mean(z)	σ_z	mean(roll)	σ_{roll}	mean(pitch)	σ_{pitch}	mean(yaw)	σ_{yaw}
A1	-0.01 m	0.35 m	2.73 m	0.44 m	0.06 m	0.18 m	1.90°	5.74°	2.08°	4.53°	183.28°	3.75°
A2	-0.03 m	0.31 m	2.77 m	0.39 m	0.07 m	0.19 m	3.47°	6.05°	2.68°	4.94°	182.55°	3.90°
A3	0.04 m	0.34 m	2.77 m	0.37 m	0.06 m	0.18 m	1.64°	5.10°	1.99°	4.73°	182.66°	3.28°
A4	-0.00 m	0.26 m	2.72 m	0.33 m	0.07 m	0.21 m	1.78°	5.00°	4.04°	4.73°	180.72°	3.63°
A5	-0.06 m	0.27 m	3.73 m	0.33 m	0.06 m	0.23 m	0.64°	4.90°	0.85°	4.47°	183.91°	2.10°
R1	-0.01 m	0.54 m	3.62 m	0.17 m	-0.01 m	0.11 m	1.63°	4.21°	1.44°	2.04°	183.70°	3.76°
R2	-0.03 m	0.52 m	3.76 m	0.39 m	-0.04 m	0.19 m	2.59°	3.89°	0.57°	2.53°	183.39°	4.00°
R3	-0.07 m	0.28 m	2.02 m	0.31 m	0.04 m	0.13 m	1.49°	6.75°	4.24°	3.68°	181.44°	5.38°
L1	-0.01 m	0.36 m	3.70 m	0.31 m	0.07 m	0.19 m	0.69°	6.11°	3.72°	4.35°	181.47°	2.39°
M1	-0.08 m	0.29 m	2.71 m	0.26 m	0.05 m	0.16 m	0.38°	3.48°	4.26°	2.74°	179.91°	1.93°
M2	-0.14 m	0.37 m	3.70 m	0.23 m	0.06 m	0.21 m	1.52°	4.90°	3.62°	3.04°	180.30°	3.62°

encoded in our framework, it provided an additional source of error.

V. CONCLUSIONS

In this paper, the use of on-board inexpensive cameras to derive the relative pose between two flying vehicles, was utilized to enable autonomous formation flying capabilities. A unique feature of the relative localization technique (the symmetry of α and β angles extraction) helped to quickly prune outliers. The performance of the proposed approach

was assessed for various trajectories, both indoors and outdoors. Future work will entail the utilization of the ego-motion estimates from inertial and altitude sensors as well as from a Visual Odometry setup. The collected information will be fused in a Bayesian probabilistic framework such as an extended Kalman filter (based on our analytical solution.) More precise ground-truth is also planned.

Because of the low weight requirement of our approach, it is currently being tested on under-actuated cubic blimps that move at slow speeds [36]; see Fig. 6. Applications
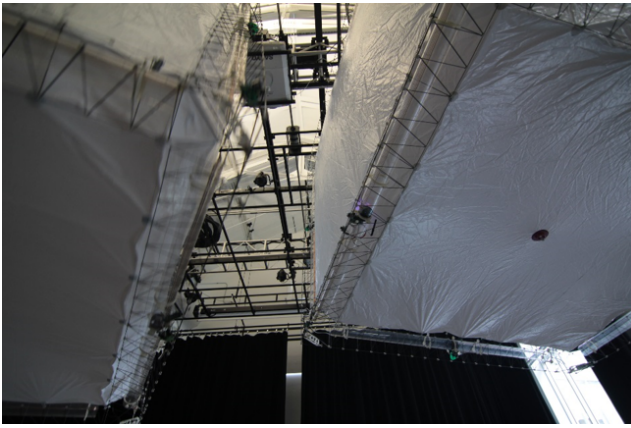
Fig. 6.   Two Tryphon Blimps flying while observing each other.

to underwater vehicles [37] are also considered, since they are generally deployed in unstructured, GPS-denied environments. Finally, the use of omni-directional or extreme wide angle cameras would further improve the sensing capabilities and allow more than two robots to operate together.

REFERENCES

[1] D. Mellinger, N. Michael, M. Shomin, and V. Kumar, "Recent advances in quadrotor capabilities," in *IEEE Int. Conf. on Robotics and Automation*, May 2011, pp. 2964–2965.

[2] D. Mellinger and V. Kumar, "Minimum snap trajectory generation and control for quadrotors," in *Proc. IEEE Int. Conf. on Robotics and Automation*, May 2011, p. 25202525.

[3] D. Mellinger, M. Shomin, N. Michael, and V. Kumar, "Cooperative grasping and transport using multiple quadrotors," in *Int. Symposium on Distributed Autonomous Robotics Systems*, Nov. 2010.

[4] A. P. Schoellig, C. Wiltsche, and R. D'Andrea, "Feed-forward parameter identification for precise periodic quadrocopter motions," in *American Control Conf.*, 2012, pp. 4313 – 4318.

[5] F. Augugliaro, A. Schoellig, and R. D'Andrea, "Dance of the Flying Machines: Methods for Designing and Executing an Aerial Dance Choreography," *IEEE Robotics Automation Magazine*, vol. 20, no. 4, pp. 96–104, Dec 2013.

[6] D. Brescianini, M. Hehn, and R. D'Andrea, "Quadrocopter pole acrobatics," in *IEEE/RSJ Int. Conf. on Intelligent Robots and Systems*, Nov 2013, pp. 3472–3479.

[7] S.-M. Oh and E. N. Johnson, "Relative Motion Estimation for Vision-based Formation Flight using Unscented Kalman Filter," 2007.

[8] T. Krajník, M. Nitsche, J. Faigl, P. Vaněk, M. Saska, L. Přeučil, T. Duckett, and M. Mejail, "A Practical Multirobot Localization System," *Journal of Intelligent and Robotic Systems*, vol. 76, no. 3-4, pp. 539–562, 2014. [Online]. Available: http://dx.doi.org/10.1007/s10846-014-0041-x

[9] R. Tron, J. Thomas, G. Loianno, J. Polin, V. Kumar, and K. Daniilidis, "Vision-Based Formation Control of Aerial Vehicles," in *Workshop on Distributed Control and Estimation for Robotic Vehicle Networks*, 2014.

[10] T. Nageli, C. Conte, A. Domahidi, M. Morari, and O. Hilliges, "Environment-independent formation flight for micro aerial vehicles," in *IEEE/RSJ Int. Conf. on Intelligent Robots and Systems*, Sept 2014, pp. 1141–1146.

[11] M. Faessler, E. Mueggler, K. Schwabe, and D. Scaramuzza, "A Monocular Pose Estimation System based on Infrared LEDs," in *IEEE Int. Conf. on Robotics and Automation*, 2014.

[12] K. E. Wenzel, A. Masselli, and A. Zell, "Visual Tracking and Following of a Quadrocopter by another Quadrocopter," in *IEEE/RSJ Int. Conf. on Intelligent Robots and Systems*, 2012.

[13] J. J. Lugo, A. Masselli, and A. Zell, "Following a quadrotor with another quadrotor using onboard vision," in *European Conf. on Mobile Robots (ECMR)*, 2013.

[14] O. Dugas, P. Giguère, and I. Rekleitis, "6DoF Camera Localization for Mutually Observing Robots," in *Int. Symposium on Robotics Research ISRR*, Singapore, Dec. 2013.

[15] P. Giguere, I. Rekleitis, and M. Latulippe, "I see you, you see me: Cooperative Localization through Bearing-Only Mutually Observing Robots," in *IEEE/RSJ Int. Conf. on Intel. Robots and Systems,*, Portugal, Oct. 2012, pp. 863–869.

[16] G. Klein and D. Murray, "Parallel tracking and mapping for small AR workspaces," in *Proc. Sixth IEEE and ACM Int. Symposium on Mixed and Augmented Reality (ISMAR'07)*, Nara, Japan, November 2007.

[17] J. Engel, J. Sturm, and D. Cremers, "Scale-Aware Navigation of a Low-Cost Quadrocopter with a Monocular Camera," *Robotics and Autonomous Systems (RAS)*, vol. 62, no. 11, pp. 1646–1656, 2014.

[18] ——, "Accurate Figure Flying with a Quadrocopter Using Onboard Visual and Inertial Sensing," in *Proc. of the Workshop on Visual Control of Mobile Robots (ViCoMoR) at the IEEE/RJS Int. Conf. on Intelligent Robot Systems (IROS)*, Oct. 2012.

[19] ——, "Camera-Based Navigation of a Low-Cost Quadrocopter," in *Proc. of the Int. Conf. on Intelligent Robot Systems*, Oct. 2012.

[20] R. Kurazume, S. Nagata, and S. Hirose, "Cooperative positioning with multiple robots," in *IEEE Int. Conf. on Robotics and Automation*, vol. 2, 1994, pp. 1250–1257.

[21] R. Kurazume and S. Hirose, "An experimental study of a cooperative positioning system," *Autonomous Robots*, vol. 8, pp. 43–52, 2000.

[22] I. Rekleitis, G. Dudek, and E. Milios, "Experiments in free-space triangulation using cooperative localization," in *IEEE/RSJ/GI Int. Conf. on Intel. Robots and Systems*, 2003, pp. 1777–1782.

[23] S. Roumeliotis and G. Bekey, "Collective localization: A distributed kalman filter approach to localization of groups of mobile robots," in *IEEE Int. Conf. on Robotics and Automation*, 2000, pp. 2958–2965.

[24] S. Roumeliotis and G. A. Bekey, "Synergetic localization for groups of mobile robots," in *Proceedings of the 39th IEEE Conf. on Decision and Control*, vol. 4, 2000, pp. 3477–3482.

[25] I. Rekleitis, G. Dudek, and E. Milios, "Probabilistic cooperative localization and mapping in practice," in *IEEE Int. Conf. on Robotics and Automation*, 2003, pp. 1907–1912.

[26] A. Franchi, P. Stegagno, and G. Oriolo, "Probabilistic mutual localization in multi-agent systems from anonymous position measures," in *49th IEEE Conf. on Decision and Control*, Dec. 2010, pp. 6534–6540.

[27] N. Trawny, X. Zhou, K. Zhou, and S. Roumeliotis, "Interrobot Transformations in 3-D," *IEEE Transactions on Robotics*, vol. 26, no. 2, pp. 226–243, April 2010.

[28] X. Zhou and S. Roumeliotis, "Determining the robot-to-robot 3D relative pose using combinations of range and bearing measurements: 14 minimal problems and analytical solutions to 3 of them," in *Proc. IEEE/RSJ Int. Conf. on Intel. Robots and Systems*, 2010, pp. 2983–2990.

[29] ——, "Determining the robot-to-robot 3D relative pose using combinations of range and bearing measurements (part ii),," in *Proc. IEEE Int. Conf. on Robotics and Automation*, Shanghai, China, 2011, pp. 4736–4743.

[30] ——, "Determining 3D relative transformations for any combination of range and bearing measurements," *IEEE Transactions on Robotics*, 2012.

[31] B. Weber, P. Zeller, and K. Kuhnlenz, "Multi-camera based real-time configuration estimation of continuum robots," in *IEEE/RSJ Int. Conf. on Intel. Robots and Systems*, 2012, pp. 3350–3355.

[32] R. Kennedy, K. Daniilidis, O. Naroditsky, and C. Taylor, "Identifying maximal rigid components in bearing-based localization," in *IEEE/RSJ Int. Conf. on Intel. Robots and Systems*, 2012, pp. 194–201.

[33] O. Naroditsky and K. Daniilidis, "Optimizing polynomial solvers for minimal geometry problems," in *IEEE Int. Conf. on Computer Vision*, 2011, pp. 975–982.

[34] V. Dhiman, J. Ryde, and J. J. Corso, "Mutual Localization: Two Camera Relative 6-DOF Pose Estimation from Reciprocal Fiducial Observation," arXiv preprint arXiv:1301.3758, 2013.

[35] M. Monajjemi, "ROS driver for Parrot AR-Drone quadrocopter," https://github.com/AutonomyLab/ardrone_autonomy, 2014.

[36] I. Sharf, M. S. Persson, D. St-Onge, and N. Reeves, "Development of aerobots for satellite emulation, architecture and art," in *Proc. the 13th Int. Symp. on Experimental Robotics*, 2012.

[37] G. Dudek, M. Jenkin, C. Prahacs, A. Hogue, J. Sattar, P. Giguere, A. German, H. Liu, S. Saunderson, A. Ripsman, S. Simhon, L.-A. L-A Torres, E. Milios, P. Zhang, and I. Rekleitis, "A visually guided swimming robot," in *IEEE/RSJ Int. Conf. on Intel. Robots and Systems*, 2005, pp. 3604–3609.